European Journal of Pharmaceutics and Biopharmaceutics 78 (2011) 196–207

Contents lists available at ScienceDirect

European Journal of Pharmaceutics and Biopharmaceutics

journal homepage: www.elsevier.com/locate/ejpb

Research paper

Addressing new analytical challenges in protein formulation development

Henryk Mach [a,*], Tudor Arvinte [b,c]

[a] Merck Research Laboratories, Merck & Co., West Point, USA
[b] Department of Pharmaceutics and Biopharmaceutics, University of Geneva, Geneva, Switzerland
[c] Therapeomic Inc., Basel, Switzerland

ARTICLE INFO

Article history:
Available online 8 March 2011

Keywords:
Therapeutic proteins
Formulation
Spectroscopic methods
Phase separation
Flow cytometry
Analytical ultracentrifugation

ABSTRACT

As the share of therapeutic proteins in the arsenal of modern medicine continue increasing, relatively little progress has been made in the development of analytical methods that would address specific needs encountered during the development of these new drugs. Consequently, the researchers resort to adaptation of existing instrumentation to meet the demands of rigorous bioprocess and formulation development. In this report, we present a number of such adaptations as well as new instruments that allow efficient and precise measurement of critical parameters throughout the development stage. The techniques include use of atomic force microscopy to visualize proteinacious sub-visible particles, use of extrinsic fluorescent dyes to visualize protein aggregates, particle tracking analysis, determination of the concentration of monoclonal antibodies by the analysis of second-derivative UV spectra, flow cytometry for the determination of subvisible particle counts, high-throughput fluorescence spectroscopy to study phase separation phenomena, an adaptation of a high-pressure liquid chromatography (HPLC) system for the measurement of solution viscosity and a variable-speed streamlined analytical ultracentrifugation method. An ex vivo model for understanding the factors that affect bioavailability after subcutaneous injections is also described. Most of these approaches allow not only a more precise insight into the nature of the formulated proteins, but also offer increased throughput while minimizing sample requirements.

1. Introduction

The success of several of therapeutic proteins that were introduced throughout the last decade of the 20th century resulted in an exponential growth of interest in the development of new biological drugs [1]. The majority of the global pharmaceutical companies that focused on small molecule drugs presently shift a substantial portion of their resources into biological products, whose dominance in the field of novel pharmaceuticals becomes apparent. The intensity and breath of the research is creating new analytical challenges, due to the sheer number of samples that need to be simultaneously analyzed and compounding factors such as highly concentrated samples that contain variety of excipients [2–4]. To date, some of these challenges have been satisfactorily met by instrument manufacturers [2,5–7]. In most cases, new aspects of the formulated protein samples are being analyzed, but typically both the measurement and subsequent data analysis are performed sequentially by the operator. One technique that has been developed some time ago, but is now attracting renewed interest due to capability of analyzing sub-micron and sub-visible particles is asymmetric flow field-flow fractionation [8–10]. However, it typically requires extensive method development due to the complexity of the observed interactions. Imaging techniques introduced to address the problem of the presence of particulates are micro-flow imaging (MFI) [5,11] and particle tracking analysis (PTA) [6,7], the latter discussed in more detail later in this text. Both techniques have limitations related to the size range that can be analyzed. Micro-flow imaging most often is used to detect particles larger than 2 μm, and particle tracking analysis works in a very narrow concentration range of particles smaller than 1 μm. Additionally, in both cases the measurements are performed sequentially by the operator. The existing characterization techniques employed in protein formulation development typically describe only a range of properties (e.g. Mw and size) thus necessitating the development of new tests for comprehensive testing of samples. In a typical industrial environment, where multiple projects are underway simultaneously, the requirement for high throughput is paramount [12,13]. Additionally, often these projects are in early stages of development, and the amount of material is limited. Thus, the emphasis is also on minimization of the sample size. In this report, we describe a number of adaptations that were performed to answer specific analytical needs in protein formulation development. They show that the practical use of existing hardware, when supplemented with the use of available software

* Corresponding author. Merck Research Laboratories, WP78-302, West Point, Pennsylvania, USA. Tel.: +1 215 652 4689.
E-mail address: henryk.mach@merck.com (H. Mach).

0939-6411/$ - see front matter © 2011 Elsevier B.V. All rights reserved.
doi:10.1016/j.ejpb.2011.03.001

capabilities, often can address the needs of protein formulation development.

2. Determination of morphology of proteinacious subvisible particles by atomic force microscopy

The presence of protein aggregates attracts great attention of therapeutic protein formulators due to the potential adverse effects on safety and efficacy [14,15]. Therefore, their amount, size, structure, and reversibility are important parameters that affect the formulation process [16–19]. However, most of the biophysical instruments available focus on structural changes, reflecting the focus of scientific research in the past decades [20–23]. Consequently, little has been known about morphology of monoclonal antibody (mAb) aggregates. Widely used technique for aggregation (as well as fragmentation) assessment, size-exclusion chromatography [24], results in the loss of the majority of sub-micron and essentially all subvisible (<75 μm) as well as visible aggregates, due to the surface binding in the preparative steps or on the column [8]. Other techniques that have been used with varying degrees of success in the analysis of aggregates [2] also did not provide any direct information about morphology of the particles. Newer techniques, such as flow imaging [5,11,25], do not have sufficient resolution to probe structural organization of aggregates on a sub-micron scale. On the other hand, atomic force microscopy, while immensely popular in nanotechnology fields [26,27], seldom has been used to visualize protein aggregates [28–31], despite resolution approaching several nanometers. The use of transmission electron microscopy (TEM), while affording excellent resolution, typically is performed only on select samples and can potentially introduce artifacts due to chemical staining [9].

Monoclonal antibodies present a special case, since they have two identical domains (Fabs) attached to a common root (Fc). The presence of multiple sites that may potentially engage in oligomerization network is an essential prerequisite in the *modus operandi* of neutralizing monoclonal antibodies [32]. In principle, the aggregate growth can occur though either a recruitment of a monomer to already existing aggregate or through a coalescence of two separate aggregates. In a simplified aggregation model, each Fab contains one specific hydrophobic *locus* on its surface, which is capable of irreversibly attaching to the identical spot on another molecule of its kind. The flexibility of hinge regions will result in a capability to bind to another aggregation-prone spot on the same oligomer. Assuming lack of prohibitive spatial hindrance, the self-association will be much more likely than recruitment of another molecule due to the extremely high local concentration resulting from the membership in the same oligomeric particle. In order to examine the morphology of mAb aggregates by AFM at molecular level, a sample of therapeutic mAb was placed on a mica disk pretreated with a solution of poly-lysine. The antibodies were allowed to bind to the disk and be visualized by atomic force microscope after drying. In solution, this mAb showed tendency to self-associate in a manner leading to distinct opalescence that seemed to be proportional to the ionic strength of the formulation (not illustrated). Indeed, AFM image (Fig. 1) reveals the presence of clusters of oligomers. These oligomers are approximately 50 nm in diameter, while the monomers typically measure ~15 nm (as observed by AFM), and only a few such monomers are visible in the image suggesting that they do not bind readily to the mica surface [33–35]. This image presents a potential mechanism of staged mAb aggregation, where first oligomers are formed, and then they coalesce into larger assemblies. The manner of the condensation of oligomers, as well as presence or absence of oligomer formation, is dependent on the particular mAb sequence [35]. In some cases, where temperature is used to aggregate the protein, the oligomers do not form. Instead, large structures resembling "fuzzy balls" are observed that presumably are resulting from aggregation of completely unfolded molecules [35]. These results indicate that atomic microscopy can potentially unravel the propensity to form oligomeric forms that ultimately can lead to the formation of subvisible particles. Morphological evaluation can also play important role in defining structural determinants of immunogenicity and their potential clinical relevance [36–40], further increasing the potential scope of application of this technique.

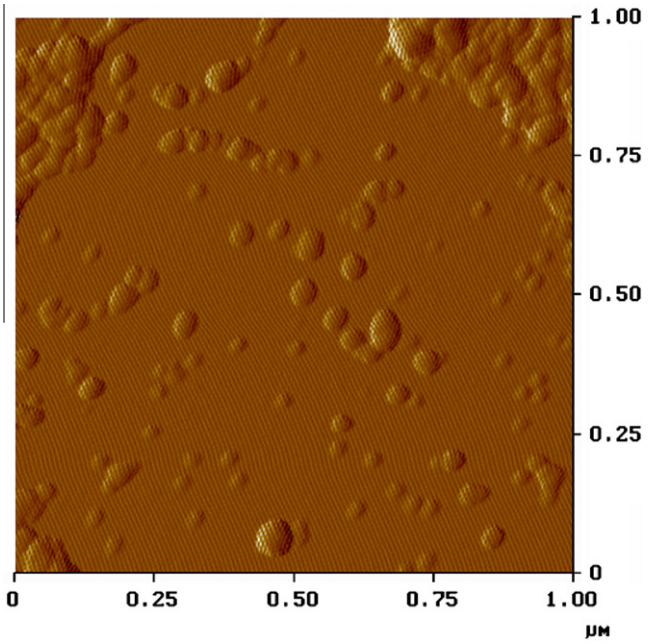

Fig. 1. Atomic force microscopy images of a monoclonal antibody. The images were prepared following a protocol described previously [35]. Briefly, prior to immobilization, the solution was subjected to 75 °C using the cuvet holder of a Jasco 750 spectrofluorometer equipped with a thermoelectric control until turbidity appeared. To pre-treat the mica disks, 10 μl of 2 mg/ml poly-L-lysine hydrochloride in water was used before antibody binding and drying. MultiModeTM scanning probe microscope from Digital Instruments interfaced on a personal computer was used. All images were taken by tapping mode at scan rate of 1.00 Hz, aspect ratio of 1:1 and tip velocity of 2.00 μm/s. (For interpretation of the references to colour in this figure legend, the reader is referred to the web version of this article.)

3. Applications of fluorescence spectroscopy to characterize therapeutic protein aggregation phenomena

The necessity of use of a battery of complementary methods to properly characterize complex protein aggregation pathways has long been postulated [41,42]. The analytical gaps become particularly acute in the case of increasingly common formulations of highly concentrated proteins [3,43,44]. Fluorescence spectroscopy, particularly in combination with microscopy, is a powerful tool often used in a spectacular manner to study biological processes occurring in living cells [45]. In the field of therapeutic protein development, it can be applied to address formulation or delivery problems affecting a number of critical quality attributes. The elusive sub-visible particles, a subject of a general debate in academic, industrial as well as regulatory circles [14,15], can be visualized by staining with a fluorescent dye [46–48], after staining with a low molecular weight phenoxazone dye, Nile Red [49,50]. Nile Red binds to hydrophobic regions of proteins that become increasingly exposed during protein unfolding, or in other processes that affect the structure, such as unfavorable change of formulation parameters (e.g. pH, temperature, dielectric constant), or binding to surfaces, ligands (e.g. surfactants, buffer components), and other

proteins [9,46,50]. The intense fluorescence that Nile Red exhibits when in bound state has been previously exploited to characterize calcitonin fibrillation [51]. The use of similar dyes, such as thioflavine T, SYPRO Orange, bis-ANS (4,4′-bis-1-anilinenaphtalene 8-sulfonate), and DCVJ (4-dicyanovinyl julolidine) typically yield similar results when used for the characterization of the extent and dynamics of protein aggregation [52]. The sensitivity of the detection of aggregate formation using Nile Red staining is illustrated in Fig. 2. Even though no signal increase in terms of fluorescence intensity or UV absorbance is detected for first two hours, the images of Nile Red-stained sample reveals gradual appearance of small bright objects that represent growing aggregates [46]. These aggregates are, however, very small in numbers, so they are not detectable by UV or Nile Red spectroscopy. At approximately 2 h, the fluorescence signal begins to rise, while the UV signal still remains unchanged, demonstrating superior sensitivity of the fluorescence detection. At that point, with UV signal still unchanged, a large number of dye-stained aggregates of various sizes are apparent in the microscope image. In addition to serving as a visualization tool, the emission originating from stained aggregates can be utilized by other classical fluorescence techniques. For example, the steady-state fluorescence intensity is indicative of the degree of dye binding even in the absence of aggregates that can be visually detected [9,46,53]. Additionally, fluorescence polarization and fluorescence lifetime measurements allow the estimation of rotational dynamics of fluorescent moieties inside of protein aggregates [9,47,54,55]. Similarly, measuring time decay of the fluorescence after pulsed excitation permits the determination of the lifetime of the excited state that is dependent on the microenvironment of the probed chromophore [54]. Finally, the scattered, rather than fluorescent, light can also be efficiently detected by detectors in fluorescence instruments, providing a very sensitive measure of the onset of protein aggregation [46]. Moreover, collection of the light scattering signal as a function of the excitation wavelength (light scattering spectra) allows reliable comparison of the degree of aggregation [46].

4. An ex vivo model for interactions of monoclonal antibodies with subcutaneous tissue

Most of the subcutaneously injected monoclonal antibodies currently in use exhibit modest bioavailability, typically in the 50–65% range. Despite the staggering cost of goods for these highly concentrated biological products [3], the exact fate of the lost material is not known. This is a situation where new experimental approaches need to be created in order to advance the formulation science to the ultimate benefit of the patient. Obviously, animal experiments, while being most relevant, suffer from high variability, difficulty measuring drug concentrations at various points of the subcutaneous delivery route, contamination with body fluids, and a host of other analytical challenges. Alternatively, the subcutaneous tissue can be excised and then controlled ex vivo binding experiments performed to elucidate the parameters that affect the extent of loss at the subcutaneous injection site.

The lymphatic absorption is the predominant route of protein drugs absorption due to their size [56–58], with external factors such as heat [59], exercise [60], massage [61] also affecting absorption kinetics. The separated rat subcutaneous tissue can be homogenized after freezing using a common household coffee grinder, and water slurries of such homogenized material stored for subsequent studies [62]. Incubation of the homogenized rat tissue with monoclonal antibodies under various formulation conditions results in partial binding of the antibodies. The extent of binding can be measured quantitatively by subjecting centrifuged supernatants to size-exclusion chromatography analysis. Both neutral and positively charged antibodies exhibit non-specific binding (Fig. 3A). However, the presence of net positive charge appears to

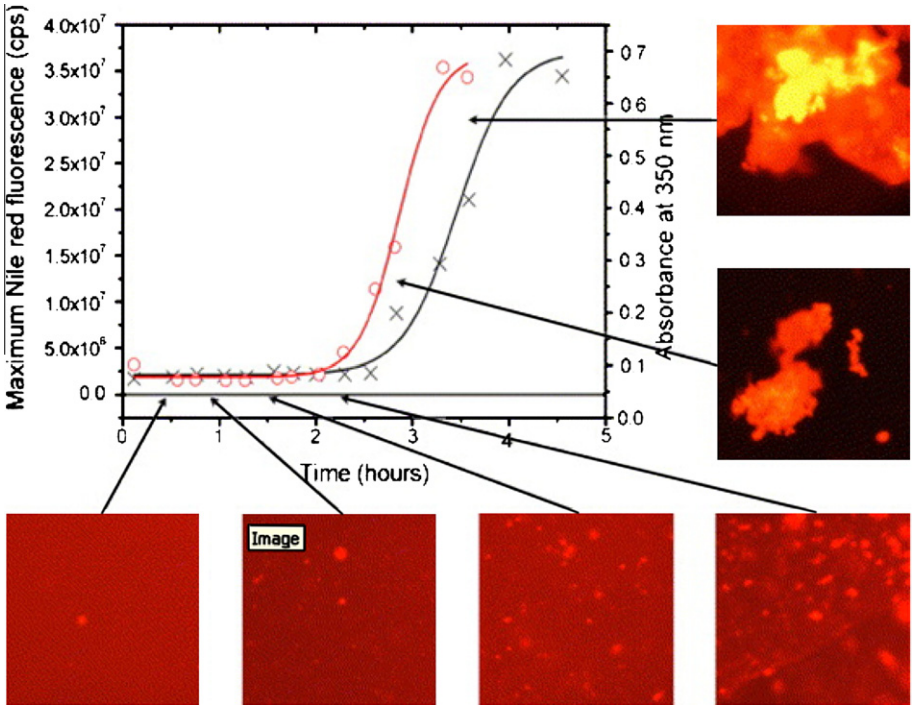

Fig. 2. Human calcitonin fibrillation in 0.05 M acetate buffer, pH 4.6, followed by microscopy, Nile Red fluorescence, and UV absorbance at 350 nm. All the data were obtained from the same solution. Nile Red fluorescence (o) detected the gelation phenomenon earlier than UV absorbance (X). Only the microscopic study of the Nile Red-stained solutions revealed that aggregates were present in the solution from the beginning and increased in number with time even in the "lag-phase". The solution finally became a turbid gel. The photomicrograph dimensions are 301 μm × 301 μm. The contrast of the first four micrographs was enhanced to allow visualization of the aggregates. (For interpretation of the references to colour in this figure legend, the reader is referred to the web version of this article.)

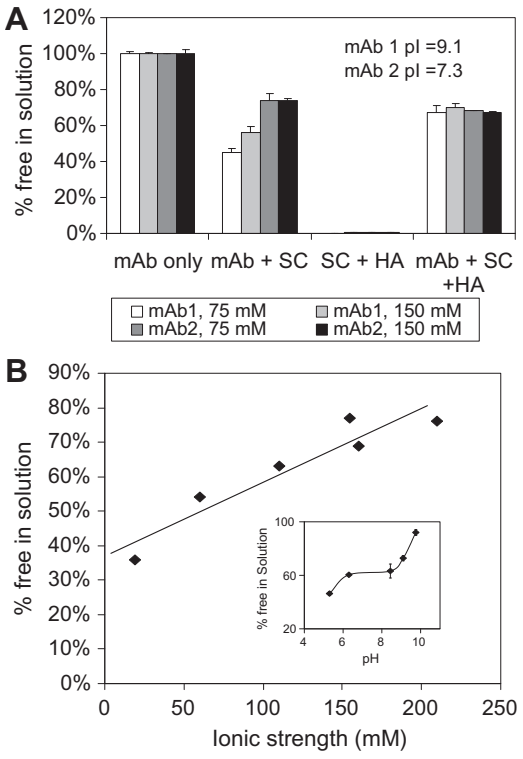

Fig. 3. Ex vivo interaction of monoclonal antibodies with rat subcutaneous tissue. (A) The effect of antibody isoelectric point and the presence of hyaluronic acid on the extent of binding to s.c. tissue. The samples were incubated in the presence of a slurry containing excised and homogenized rat subcutaneous tissue, and the amount of antibody remaining in solution was measured by size-exclusion chromatography of centrifuged and filtered supernatants. The bars within each group denote (1st) mAb 1 (pI = 9.1) in a buffer of I = 75 mM, (2nd) mAb 1 in a buffer of I = 150 mM, (3rd) mAb 2 (pI = 7.3) in a buffer of I = 75 mM, (4th) mAb 2 in a buffer of I = 150 mM. The groups of bars denote (1st) mAb only, (2nd) mAb in the presence of s.c. tissue, (3rd) s.c. tissue in the presence of hyaluronic acid (HA) with no mAb present, (4th) mAb in the presence of both s.c. and hyaluronic acid. Error bars denote standard deviation of two measurements. (B) The effect of ionic strength of the formulation on the ex vivo binding to rat subcutaneous tissue. The buffers contained either 10 mM histidine hydrochloride or 10 mM sodium phosphate (I = ~160 mM point only) at pH 6 and various amounts of sodium chloride. Inset: the effect of pH on the extent of the ex vivo binding of mAb 1 to rat subcutaneous tissue. The error bars denote average deviation of two measurements. Solid lines are present to guide the eye only. Reproduced with permission from Mach et al. [62].

increase the extent of binding to subcutaneous tissue. The electrostatic nature of the interaction is indirectly suggested by the inhibition of binding by competing hyaluronic acid, a polymer bearing high negative charge that is abundant in the subcutaneous tissue (Fig. 3A). Further indication of the electrostatic nature of the binding is given by the experiments where the dependence on ionic strength and pH was measured (Fig. 3B). While the electrostatic behavior is difficult to predict for proteins with isoelectric point between pH 6 and 8 [63], proteins of higher pI are likely to exhibit partial absorption to subcutaneous tissue. Obviously, the limited binding capacity will affect the extent of the loss for either low or high concentrations. At low doses (less than 1 mg injected at typical volume of few hundred microliters), significant loss is expected that should be taken into account when interpreting pharmacokinetic data from dose-ranging studies. Conversely, at high doses (>50 mg injected), the local loss to the subcutaneous tissue is expected to be insignificant, due to limited spatial distribution of the injected volume [64] in the absence of added hyaluronidase [65]. These experiments, despite being successful in identifying small, but measurable effect of electrostatic binding to the subcutaneous tissue, failed to explain why highly concentrated, neutrally charged monoclonal antibody still exhibits limited (~62%) bioavailability in humans [66]. One plausible explanation is that significant pinocytosis occurs during the days that are needed to reach the general circulation, and the overload of neonatal FcRn receptors results in excessive endosomal degradation of the protein traveling through lymphatics [67–69]. Nevertheless, for proteins delivered at relatively small doses, especially those bearing positive charge, the rat ex vivo model may be a useful tool in the development of optimal formulation and delivery protocols.

5. Multicomponent analysis of second-derivative UV spectra for protein concentration determination

The determination of protein concentration based on the absorbance value at 280 nm is one of the most often performed tasks in the formulation practice. This seemingly simple operation, however, is ridden with potential pitfalls. First, a correct value of the extinction coefficient needs to be known. At the early stages of formulation development, the value needs to be calculated, or, if sufficient amount of sample is available, determined from measurements in 6 M guanidine–HCl, where complete denaturation removes the effect of local micro-environments on the intensity of spectral bands. For the calculation approach, the extinction coefficient values for tryptophan, tyrosine, and cystine in "average protein" have been determined [70], and later confirmed using a larger data set [71]. Monoclonal antibodies, however, due to the presence of solvent-exposed so-called complementarity-determining regions (CDRs), tend to contain a disproportional number of solvent-exposed tyrosine side chains, and, consequently, the equation for the calculation of molar extinction coefficients of monoclonal antibodies in native buffers is as follows [72]:

$$\varepsilon_{280\text{nm}} = 5540^{*}\text{TRP} + 1400^{*}\text{TYR} + 125^{*}\text{CYS} \quad (1)$$

where $\varepsilon_{280\text{nm}}$ is the molar extinction coefficient of a monoclonal antibody (IgG1 or IgG2) expressed per mole per 1-cm path length (M^{-1} cm^{-1}), TRP, TYR, and CYS are the numbers of tryptophan, tyrosine, and cystine (S–S bonds), respectively. In the "average" protein, the value of the extinction coefficient of tyrosine is 1480 M^{-1} cm^{-1} instead of 1400 M^{-1} cm^{-1} [70].

When the value of the extinction coefficient is known, the concentration of the measured samples can be precisely determined, provided that appropriate corrections related to the baseline and the presence of light scattering are made. In most cases, the logarithmic fitting procedure [70,73,74], often provided with the instruments' controlling software package, can be applied.

Once the concentration of the first purified sample is determined with sufficient degree of accuracy, the subsequent measurements can be expedited with increased assurance of artifact-free data, by calculating a second-derivative spectrum and performing a variance-weighted least-squares fit to the original spectrum ("standard") of known concentration that was previously acquired [72]. The second-derivative spectra of a monoclonal antibody, the "standard" one used for concentration determination, and the fitted one are shown in Fig. 4A. Fig. 4B shows the results of multicomponent analysis of the second-derivative spectra of a serially diluted concentrated monoclonal antibody. It is apparent that reasonable results have been obtained up to concentrations of 10 mg/ml, much higher in comparison with the conventional $A_{280\text{nm}}$ method. The multicomponent analysis method has been also more accurate at the low concentration range (0.01–0.1 mg/ml). The underlying reason of increased precision and accuracy is twofold. First, multiple data points are taken into account, providing data averaging that improves the precision. Second, these data points are weighted according to the standard deviation. The diode-array instruments pass the entire beam through the sample before

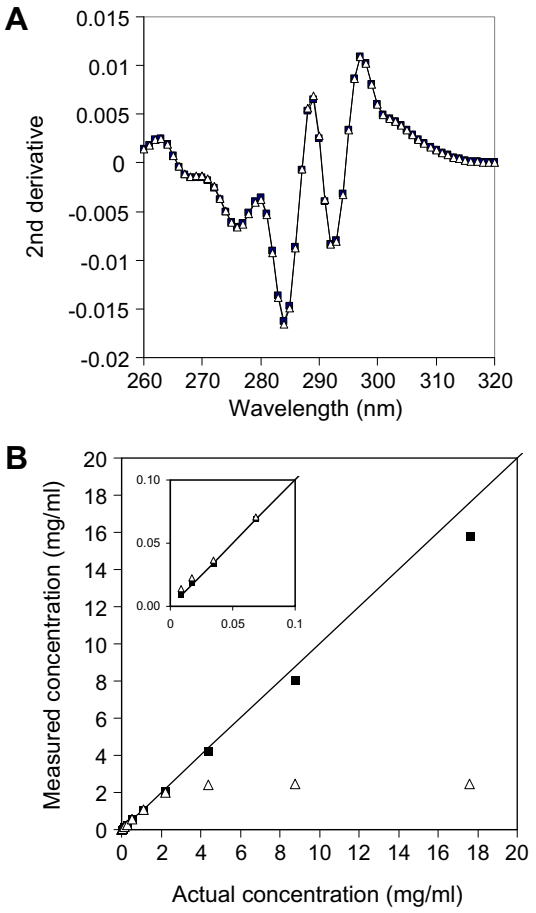

Fig. 4. (A) Second-derivative spectra of a monoclonal antibody sample (solid squares) and the fitted standard (open triangles). The concentration of the antibody was 1.06 mg/ml. (B) Multicomponent analysis of a monoclonal antibody sample. Monoclonal antibody was serially diluted in phosphate buffered saline and measured by multicomponent analysis (filled squares). The results from a conventional A280 analysis are also shown (open triangles). The inset shows a magnification of the 0–0.1 mg/ml region of the plot. The solid line depicts the $Y = X$ line. Reproduced with permission from Mach and Middaugh [72].

splitting the beam onto an array of diodes. Consequently, a typical measurement comprises an average of multiple split-second readings, generating standard deviation at each data point. When the absorbance becomes too high, as is the case for concentrated proteins near 280 nm, more weight is put into the spectral regions where signal is optimal, thus increasing the accuracy of the procedure. At low concentrations, where the small vertical deviations (baseline offsets) are often observed to various degrees in everyday practice, the use of second derivatives typically results in better accuracy. Additionally, both the light scattering and vertical offset resulting from imperfections in the light path have negligible curvatures, when probed locally in the spectrum. Therefore, they can be approximated by a straight line, which does not have any contributions to the second-derivative spectra. Since the sequence of steps invoking the multicomponent analysis can be typically preprogrammed in the instruments' controlling software, a number of samples can be analyzed simultaneously, further streamlining the operations.

The ability of the second derivative approach to partially negate signal saturation artifacts due to high concentration does not imply that it is the recommended approach for highly concentrated samples. A number of short path length cells are available, at path lengths as short as 8 μm. Some cells can be disassembled between the measurement for easy cleaning and introduction of viscous samples (Hellma Gmbh & Co. KG, Mullheim, Germany, www.hellma-analytics.com). The difficulties in determining the exact path length in the measurements of highly concentrated protein solutions can be overcome by performing measurements at precisely controlled path intervals, starting at pathlengths as short as 10 μm, with a resolution of 5 μm. Using a dedicated attachment to the Varian Cary 50 Spectrophotometer (Agilent, Inc., Santa Clara, CA) allows collection of precise and reproducible data for protein concentrations exceeding 100 mg/ml (C-Technologies, Bridgewater, NJ, www.solovpe.com). The attachment can be connected to the Cary 50 UV spectrophotometer through fiber optics. A computer-controlled drive moves the tip of the fiber optic surface through the protein solution contained in a cylindrical cuvet. In such arrangement, a plot of absorbance vs. path length is constructed. Knowing the extinction coefficient, the concentration of the sample can be determined.

6. Characterization of the sub-micron macromolecules by particle tracking system

Nanoparticle tracking analysis (NTA) uses arrangement that is similar to dynamic light scattering [75] in terms of the dimensions of the observation volume and the illuminating laser. However, instead of measuring intensity fluctuations of the whole sample and determining sizes from the autocorrelation function, NTS instrument measures the Brownian motion of each individual particle. Short movies recorded by the instrument [7] are analyzed by a specialized software that tracks individual particles and calculates their diffusion coefficients. An example of output from the system is shown in Fig. 5. Typical images acquired by the system is shown in the left panel, indicating limitations of the system. The concentration of particles must fall in a narrow range to assure satisfactory sampling and at the same time prevent overcrowding that would make it difficult to follow individual particles. The right panel shows the distribution of the particles whose motions have been measured and hydrodynamic radii calculated. Indeed, the technique accurately measures about equal numbers of 100 nm and 200 nm polystyrene beads that were present in the sample. As expected, the same solution, when examined by dynamic light scattering, presents only the larger (i.e. 200 nm) population, due to known dependence of intensity on the molecular weight of the particles [72]. It should be noted, however, that the total particle concentration should be in the range between 10^7 and 10^9 particles/ml to properly populate the observation window of the instrument [7]. In summary, particle tracking analysis offers unique ability to measure the size of individual particles in solution making it independent of many limitations that characterize related techniques [75].

7. Detection of subvisible particles in therapeutic protein formulations by flow cytometry

The gap in the size range that leads to frequent overlooking of the subvisible particles smaller than 2–10 μm has been a subject of discussion of formulation scientists in both the academic and industrial circles [14,15]. Several new instruments appeared that at least partially fill the gap. Micro-flow imaging, an instrument comprising a flow cell, and a microscope-based imaging system has become a standard for the determination of size distributions of therapeutic proteins [5,11,25]. Yet, the system is operated sequentially, sample requirement is fairly large (~0.5–1.0 ml), and most importantly, the detection limit in practice is approximately 2 μm. Particle tracking systems, on the other hand, can detect and size particles in the 50 nm–1 μm range, but the observation volumes are exceedingly small, precluding statistically

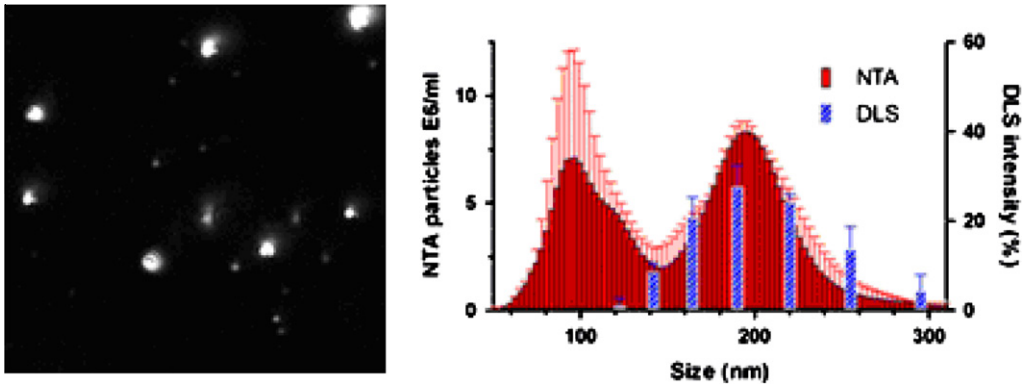

Fig. 5. The size distribution from NTA and DLS measurements of mixtures of monodisperse polystyrene beads, equal numbers of 100 nm and 200 nm diameter beads, (right panels), with the corresponding NTA video frame (left panel). Reproduced with permission from Filipe et al. [7].

significant sampling of protein particulates [6,7]. With these limitations in mind, the potential of flow cytometry appears to be compelling. The detection limit appears to be 1 μm under practical settings used to detect subvisible particles, the sample volume is optimal (~50 μl) for the capture of sufficient subvisible particles for a statistically significant result, the protein particles are routinely stained for differentiation from contaminating "dust", and the system is run in a high-throughput mode due to presence of a 96-well autosampler [76]. In a typical flow cytometer, an aqueous sheath of fluid flows through a flow cell, and the sample flow is injected into the center of the flowing fluid at a slower pace, resulting in a "single file" alignment of the particles in the focus zone, where the detection occurs. Typically forward and size scattering signals, and a number of fluorescence signals are being collected, allowing detection and categorization of particles according to their fluorescent and light scattering properties. One issue that can be addressed by flow cytometry is the effect of pumping during manufacturing (e.g. filling of the vials). Typical output of such an experiment is shown in Fig. 6. Monoclonal antibody sample that was pumped though a piston pump was analyzed, and the results were compared to data from micro-flow imaging system. The inset shows the plots of fluorescence signal vs. side scattering. It can be seen that latex particle standards are not fluorescent, and 1 μm standard is at the far left position, while the 5 μm standard is at far right – defining the size range that can be qualitatively assessed from these plots. The vertical scales of the plots in the inset reflect the fluorescence of the samples – in the case of protein particles the fluorescence originated from the SYPRO Orange, a dye that is added to each analyzed sample to differentiate protein and non-protein particles. The proportion of protein and non-protein particles appears to be constant for the samples that underwent increasing numbers of cycles in the pump. The ratio of the total count to the count obtained by micro-flow imaging was gradually decreasing as the number of passes increased. This difference can be rationalized by observing the average size growing from 1–2 μm range to >2 μm range between 1 pass and 10 pass samples (see the inset). The flow cytometry thus appears to be a promising technique that can both provide earlier warning signs of growing particle counts as well as streamline the monitoring of stability samples. In fact, it has been already successfully applied to the study of silicone oil-induced particulate formation in protein formulations [77].

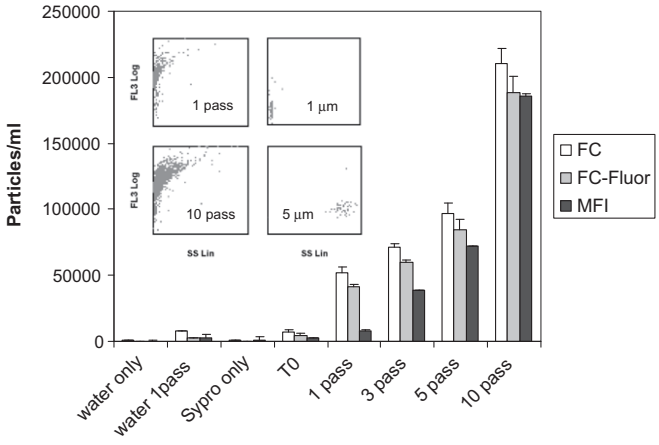

Fig. 6. The comparison of flow cytometry and micro-flow imaging based on the analysis of a monoclonal antibody samples after piston pump treatment. The protein (~5 mg/ml) was subjected to 1, 3, 5, and 10 passes through a piston pump. In each group of bars, the first bar (white) denotes total flow cytometry (FC) counts, the second bar (gray) denotes fluorescently stained particles detected by flow cytometry (FC-Fluor), and the third bar (black) denotes the particle counts (>2 μm) detected by micro-flow imaging (MFI). Error bars denote standard deviations of three measurements. Inset: SYPRO Orange fluorescence vs. side scattering intensity flow cytometry plots for 1-pass (top left) and 10-pass (bottom left) samples. One micron (top right) and 5 μm (bottom right) polystyrene standard data are shown for reference. Reproduced with permission from Mach et al. [76].

8. Simultaneous determination of thermal unfolding and phase separation temperatures of monoclonal antibodies formulations

The development of multiple therapeutic protein candidates in most pharmaceutical research and development laboratories throughout the industry necessitates adaptation of existing tools that would provide pertinent information in a high-throughput manner. One example of such adaptation is the use of polymerase chain reaction (PCR) instruments to study the thermal unfolding temperature of proteins that provides a high-throughput alternative for differential scanning calorimetry (DSC) and dedicated high-throughput screening fluorescence systems [78–81]. These instruments typically have efficient thermoelectric devices capable of rapid and precise temperature control in specialized blocks holding 96-well plates with small volume (e.g. 50 μl) sample wells. A fluorescence dye, instead of detecting the presence of amplified nucleotides, is used to detect binding associated with appearance of solvent-exposed hydrophobic regions after unfolding. Unfolding temperature can be measured explicitly by a number of instruments that have autosampler capability (e.g. fluorescence, DSC). However, determination of phase separation has been typically performed with only visual determination of initial opalescence and subsequent separation of the phases, often following centrifugation [82], or by UV and 90° light scattering [54,83]. The turbidity, however, results in attenuation of the fluorescence signal as well, since a portion of the emitted light is scattered instead of reaching the detector. Moreover, the opalescence and phase separation phenomena can be induced by decreasing the dielectric constant of the solvent. We have found that the use of 30% ethanol results in an onset of phase separation at temperatures and concentrations that can be easily achieved in a typical experiment, approximately 10 °C at 10 mg/ml. The suppression of thermal unfolding temperature occurs, but it is still about 20° higher than the phase separation temperature, assuring that the phase separation phenomena occur while the protein is in the folded state. Moreover, for six monoclonal antibodies tested, the slope of suppression of unfolding temperature as a function of ethanol concentration was essentially the same, approximately 20 °C from 0% to 30% ethanol (H. Mach, unpublished results). An example of data obtained by this approach is shown in Fig. 7. A monoclonal antibody was subjected to thermal melts in the presence of 30% ethanol at formulations of various pH. Initially, fluorescence decreases as the temperature increases (panel A) due to non-specific thermal quenching. The uppermost line, corresponding to the highest protein concentration (~25 mg/ml), shows a distinctive step (a "cloud point") at approximately 15 °C, resulting from the disappearance of turbidity as the phase-separated micro-droplets dissolve. Further increase of temperature leads to unfolding of the molecule, with concomitant binding of the dye to the newly exposed hydrophobic regions. It is apparent from the graph that both "cloud point" and thermal unfolding temperatures are concentration-dependent. The data in panel A represents only one formulation with specific pH value – a serial dilution of the protein in the same buffer was placed in one column of a 96-well plate. The combined "cloud points" and unfolding transition temperatures from the entire plate comprising dilutions at various pH values are shown in panel B of Fig. 7. The concentration dependence noted in the raw data plots is apparent. It is also seen that the protein at pH 5 and pH 6 is destabilized and has increased propensity to self-associate. These results were consistent with general trends observed during long-term stability studies (not illustrated). This experiment illustrates the benefit of studying the unfolding and self-association phenomena in a high-throughput manner. It is easy to envision an experiment where dozens of different formulations are tested at an arbitrary protein concentration, following by an informed selection of conditions that would balance the stabilizing effects, with suppression of the tendency to self-associate. Since the amount of sample needed can be minimized through the use of dielectric constant modifying solvent, this approach can also be used to differentiate potential candidates at the early lead identification and optimization stages.

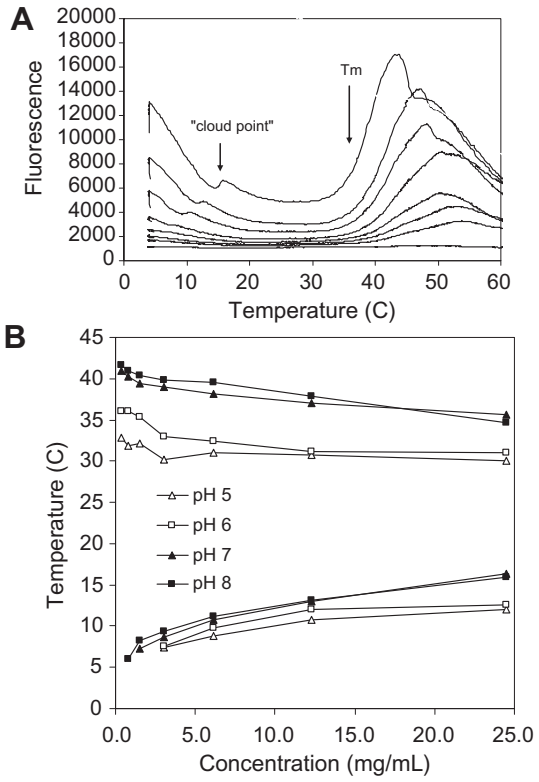

Fig. 7. The analysis of monoclonal antibody solutions at pH 7 in the presence of 30% ethanol as a dielectric constant modifier. (A) Fluorescence profiles as a function of sample temperature. 2× SYPRO Orange (Invitrogen, Carlsbad, CA) added to the samples was excited at 488 nm and the fluorescence spectra were collected. Raw data were transferred to Microsoft Excel™ workbooks for further processing (data point alignment and detection of inflection points using Visual Basic macros, emission wavelength selection and extraction). The concentrations of sample are decreasing from top to bottom, from ~25 mg/ml to ~1 mg/ml. (B) Inflection points for the "cloud points" and thermal unfolding transitions (Tm) of thermal denaturation curves as a function of protein concentration (see an example in (A)). Upper curves show Tm values and lower curves show "cloud point" values.

9. Adaptation of a high-pressure liquid chromatography system for the measurement of viscosity

With the share of subcutaneously delivered monoclonal antibodies continuously increasing, viscosity becomes the factor that limits the dose that can be safely and conveniently delivered [3,43,84]. The measurements of viscosity by the commercially available instruments involve sequential analysis of relatively large sample volumes [85–87]. Recently, a method for a high-throughput measurement assessment of small protein samples using extrinsic diffusion standards monitored by dynamic light scattering system was proposed [88], under an assumption that potential interactions of the protein with the extrinsic standards can be appropriately controlled. However, the basis for a quantitative description of viscosity, the Poiseuille's law, states linear relationship between the pressure and the viscosity of liquid under constant flow [89]:

$$\Delta P = 8\mu LQ/\pi r4 \quad (2)$$

where ΔP is the pressure drop, μ is the dynamic viscosity, L is the length of tubing, Q is the volumetric flow rate, and r is the radius of the tube. Equipment comprising an autosampler, a pump feeding the solution into small diameter tubing and a pressure sensor is readily available in essentially every laboratory in the form of a high-pressure liquid chromatography (HPLC) system. We have attached a 50-cm-long small diameter (0.005 in. ID) tubing to the output of a Waters Alliance HPLC system and recorded pressure profiles after 10 μl injections of a series of glycerol solutions (H. Mach, manuscript in preparation). The viscosities of the solutions in this study were calculated according to Chang [90]. A typical output from the pressure transducer as a function of time is shown in panel A of Fig. 8. Since a 70% glycerol solution in water (viscosity ~20 cP) is used as a running phase (and the needle washing fluid), injection of water results in a negative peak, and injection of much more viscous liquid results in a positive peak. It is also apparent that less viscous liquid diffuses faster, resulting in a broader peak. The diffusion coefficient depends not only on viscosity but also on the size of diffusing particles. Consequently, only the area under the peak was used for quantitative purposes. It should also be noted that due to the mode of operation of piston pumps, raw profiles of pressure vs. time contain pump pulse spikes. These can be removed, however, by a encoding a trivial "zapping" macro in the Visual Basic that is an integral part of each Microsoft Excel™ workbook. Fig. 8, panel B, shows the relationship of the area under the pressure peaks and the logarithm of viscosity. It appears that separate linear slopes exist for the samples that were less viscous and more viscous than the running phase. For any given HPLC system with particular tubing and temperature, calibration plots can be constructed that can subsequently be used for the ranking and potential estimation of viscosities of therapeutic protein samples. We have not observed any precipitation of concentrated monoclonal antibody samples (~200 mg/ml, ~420 cP) with the glycerol running phase (not illustrated). High precision of the results observed in these studies indicate that the parameter of viscosity that was difficult to study due to the sample and concentration requirements can now be efficiently monitored, at least in relative terms, through a high-throughput method that requires minimal amounts of sample (~10 μl vs. minimum 200 μl for conventional methods). While it was verified that correct volumes are being injected into the system for samples up to approximately 100 cP, applications where solutions of higher viscosities are typically studied may require further tests and potentially adjustments of operational parameters as needed. Prompt implementation of this method can be achieved due to the widespread availability of HPLC systems in pharmaceutical research and development laboratories. For smaller numbers of samples, a dedicated unit that measures the backpressure of flowing solution recently became available (RheoSense, San Ramon, CA, www.rheosense.com).

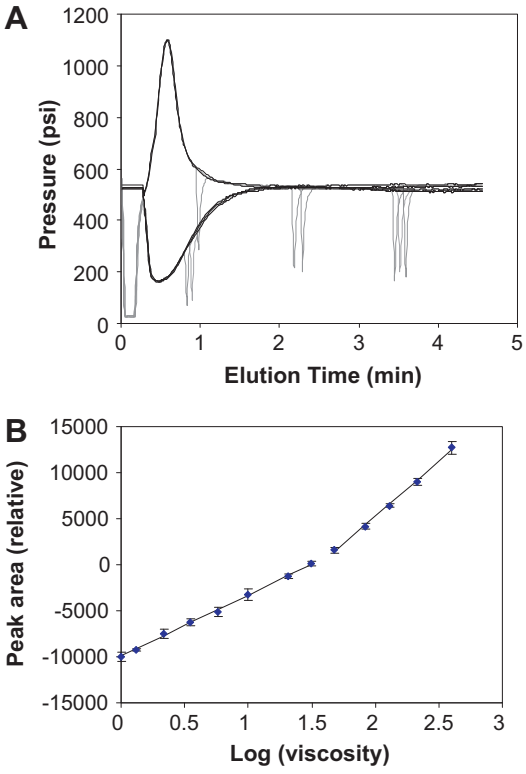

Fig. 8. (A) Representative profiles pressure vs. time profiles of glycerol standards. Gray lines show the raw data, and black lines show the profiles after digital removal of pump pulse spikes. The system was equilibrated with 70% glycerol in water as a mobile phase, and the temperature of both the sample chamber and column holder were set to 25.0 °C. The outlet flow from the HPLC pump was connected to a piece of PEEK tubing (0.005 in. inner diameter, 1/16 in. outer diameter, red-striped, Alltech), that was 50-cm long, using standard HPLC tubing connectors. The outlet of the tubing was connected to a photo-diode-array (PDA) detector for collection of UV signals to potentially estimate the concentration as well as turbidity measurements that can give the estimate of the aggregation state of tested samples. Empower 2 software (©2005, Waters Corporation) was used to run the instruments and collect the data from the 2690 series HPLC unit. The stroke volume was set 130 μL, syringe rate to "slow", depth of needle to 0, pre-column volume to 0, and needle wash time to "extended". Bubble detect and degas options were selected. High and low pressure limits were set to 4000 psi and 0 psi, respectively. The flow isocratic at 50 μL per minute, with acceleration to 10 ml/min in 2 min. The raw chromatograms were exported to a Microsoft Excel™ workbooks for further processing. (B) Calibration plot for the series of glycerol standards. Points 1–9 and 10–13 were separately fitted to a straight line by a least-squares procedure embedded in Microsoft Excel™. The error bars show the standard deviation from triplicate measurements. (For interpretation of the references to colour in this figure legend, the reader is referred to the web version of this article.)

10. Analysis of the size distribution of macromolecules by variable speed analytical ultracentrifugation

The sedimentation velocity analytical ultracentrifugation offers a unique opportunity for the study of particle size distribution due to the absence of any extraneous components in the system during analysis. However, the constant speed approach used in biological sciences limits the range of sizes that can be analyzed in a single experiment and requires considerable amount time for parameter optimization and subsequent analysis. While the concept of varying speed had been successfully introduced to the biological research by Yphantis and co-workers [91], the complexity of experimental setup and data reduction impeded the adoption of the approach. A dedicated hardware system to study colloidal systems by variable speed sedimentation was built by Machtle [92]. The system could resolve multiple species of widely varying sedimentation coefficients in up to seven samples simultaneously using an 8-hole rotor. Independently, in late the nineties a variable speed procedure was established for process and formulation development of virus-like particles. Although isolated results using this method were presented to the community soon after its development, a more detailed description was published almost a decade later, after the relevant product reached the market [93]. In the meantime, Stafford and Braswell [94] reported an application of a method using four different speeds and a part of a dedicated computer program (SEDANAL), effectively delivering an option for simultaneous analysis of species of widely varying sedimentation coefficients. The SEDANAL approach uses standard conically shaped centerpieces and traditional approach to analysis of the data that requires individual determination of menisca and selection of data ranges for analysis. However, the variable speed method

that utilizes standard 6-sector cells and automated data analysis described here may offer several advantages in some situations. The amounts of subpopulations of vastly different sizes can be assessed in a single experiment. The user involvement in data analysis is reduced to the transfer of the raw data files to an Excel™ spreadsheet. This eliminates the need for preliminary runs to establish adequate speed for particular system as well as lengthy data analysis procedures that depend on user's experience and consistency of judgment. The time required to load/unload the sample and complete analysis (excluding the time for actual run) is typically less than 30 min for nine samples, allowing a screen of 27 samples per day with total time involvement of less than 2 h. Such efficiency is often critical in pharmaceutical research laboratories, where the optimal conditions are sought for either the process or formulation, and the resolution, or even occasional artifacts are of smaller concern.

The method as described above has been found useful in situations where several species of significantly different sedimentation coefficients exist in solution. For example, it was applied in the characterization of plasmid DNA/BAK particles. BAK (benzalkonium chloride) is a positively charged surfactant that forms complexes with DNA. The dynamic light scattering data indicated that the hydrodynamic diameter of plasmid DNA was approx. 80 nm, while the DNA/BAK particles had an average of about 300 nm and higher (not illustrated). The intensity of light scattering is strongly dependent on the total molecular weight of a particle making it very difficult to detect small particles in the presence of larger sub-micron particles. The particles are also too large for conventional size analysis techniques such as gel filtration or gel electrophoresis. Employing analytical ultracentrifugation in the variable speed mode allowed rapid determination of the relative amounts of DNA present in free and particulate form. Fig. 9 (panel A) shows the changes of absorbance at reading position for samples with various BAK concentrations as a function of sedimentation coefficient value at consecutive scans. For 2 μM BAK sample, at initial slow speeds, where the value of $\log s^*$ is large minimal changes of absorbance are observed. The sharp drop in absorbance value is observed at approx. $\log s^*$ 1.3 as free DNA sediments at the corresponding centrifugal field. Increase of BAK concentration to 4 μM and 8 μM results in bimodal distribution with a subpopulation of particles sedimenting earlier at $\log s^*$ values of about 1.8. Further increase of the surfactant concentration results in the disappearance of the free DNA transition and the formation of a broad transition spanning the range between $\log s^*$ 1.5 and 3.5. At high BAK concentration (64 μM), larger particles form that sediment at lowest speed, corresponding to $\log s^*$ values of about 4. The curves in Panel A can be presented in the first derivative form (panel B). This form of presentation facilitates visual assessment of the relative concentrations of the species at various sedimentation coefficient values. For example, at 8 μM BAK, about 1/3 of DNA appears to exist as $\sim 2\log s^*$ particles, while the rest is in free state. It should be noted, however, that this analysis is approximate, since the *X*-axis scale intervals are not exactly equal (due to the arbitrarily chosen centrifugal speeds as well as different scanning times at various speeds). This is justified, as the purpose of this set up is to obtain an information about the presence of very small and very large macromolecules in one experiment in a relatively high-throughput manner.

This experimental set up has been proven to be a powerful tool in many critical junctions of pharmaceutical development, where other methods failed to adequately discern the interaction between the macromolecules. Yet, the method may appear to be flawed from theoretical point of view. For example, use of rectangular sectors in a sedimentation velocity experiment often results in convection currents that may potentially distort the resulting profiles. Very little of these artifacts have been observed, however, presumably due to a very short fraction of the total run time where any given macromolecule undergoes sedimentation. The approximate positions of the peaks were discerned nevertheless, and potential distortions of its shape were not meaningful from practical point of view. In summary, the method is found to be very useful and applied routinely to the development of biopharmaceutics.

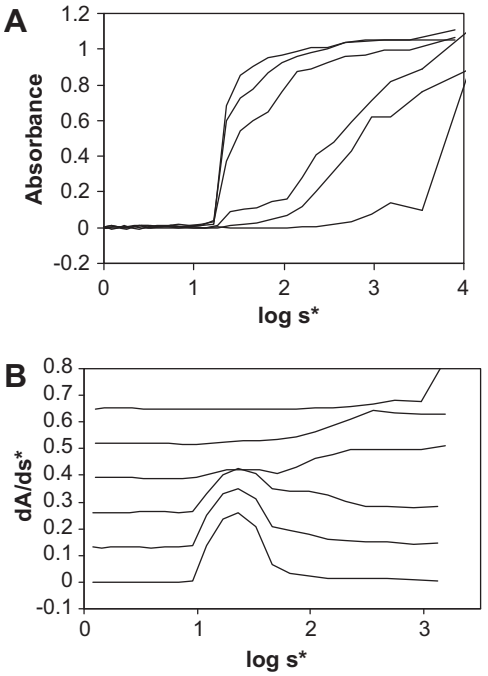

Fig. 9. (A) Absorbance values at reading position plotted versus corresponding sedimentation coefficients for DNA plasmid/ BAK mixtures at various BAK concentrations. From left to right: 2, 4, 8, 16, 32, and 64 μM BAK. DNA concentration was constant at 50 μg/ml. For the variable speed method, six-sector centerpieces were loaded with 100 μl of sample (maximum 9 samples per run) and radial scans performed using a pre-programmed method in an equilibrium step mode, 0.025 cm steps, five repetitions at increasing speeds ranging from 3000 rpm to 60,000 rpm. The speeds were (in thousands rpm): 3, 3, 3, 4, 5, 6, 7, 8, 10, 12, 14, 16, 19, 22, 25, 29, 33, 37, 41, 43, 46, 49, 52, 55, 60, 60, 60. After the run the data that consisted of cumulative $\omega 2t$ values for consecutive runs, along with radial positions and absorbance values were transferred to an Excel™ spreadsheet using a modified version of Svedberg software package [99,100]. The software that offers that option is available from the developer (http://www.jphilo.mailway.com/). Briefly, in the spreadsheet the absorbance values were extracted at radial positions that corresponded to radial distance of 0.15 cm from the meniscus, which was assumed to be constant for given cell, sector, and an exact volume (100 μl) of sample introduced. Thus, the absorbance changes at constant radial positions were observed as the centrifugal speed increased. At each speed, the corresponding sedimentation coefficient value was calculated based on the known values of cumulative $\omega 2t$, radial distance and distance from the meniscus. A plot of the first derivative of absorbance values versus the sedimentation coefficient yielded the apparent size distribution of the molecules at the scale between approximately 5 and 5000 Svedbergs. (B) First derivative plots generated from the curves in (A). The lines were offset by a constant value for clear presentation. From top to bottom: 64, 32, 16, 8, 4, and 2 μM BAK.

11. Concluding remarks

The use of comprehensive, orthogonal methods to characterize the state of therapeutic protein samples has long been postulated [2,9,14,15,42,95,96]. The existing analytical "platform" methods, however, often do not address specific aspects of the biomolecular stability in the context of particular formulation [3,42,54,97]. The current pace of the pharmaceutical development requires selection and adaptation of the existing tools for an increased analytical

throughput. The limited protein amounts that are typically available in the early stages of the development create the need to employ analytical methods that require small sample sizes.

The examples presented in this report show that in many cases the existing equipments, despite being designed for other analytical tasks, can be relatively easily adapted to provide critical information necessary for proper selection of early candidates and their formulations. In addition, new aspects of the therapeutic protein properties can be studied. For example, atomic force microscopy and electron microscopy allow the detection of aggregation intermediates, potentially linking their presence with long-term stability. HP-SEC analysis of ex vivo subcutaneous tissue samples can provide insights into the rational protein design for optimal bioavailability.

The analytical challenges of the development of highly concentrated protein biopharmaceuticals [3], measuring viscosity and propensity to self-associate, have also been addressed with appropriate methods. For protein biotherapeutics, there is also a need to analyze the aggregation states in conditions as near as possible to those the drug is applied in vivo. Sample manipulations such as dilution steps for high concentrated formulations or concentration steps for low concentrated formulations can provide misleading information on the initial aggregation state of the protein formulation [98].

In the recent years, new methods emerged that permit the characterization of size distributions of sub-micron and sub-visible particles. The use of these complementary methods strengthens the interpretation of the data and expedites optimization of the formulations, affecting not only the efficiency of the development process but also minimizing the potential of safety-related issues. The use of diversified methods is especially important in the case of heterogeneous formulations such as aggregated slow-release formulations, microparticles, or proteins absorbed onto adjuvants in vaccines. These new approaches may also be found useful in the development of new delivery devices, where material compatibility of highly concentrated proteins is essential.

In conclusion, flexibility in utilizing existing methods together with new technologies and adapting these analytical methods to the needs of the formulation contributes to an improved characterization of protein biotherapeutics.

Acknowledgements

The authors would like to thank C. Russell Middaugh for guidance through UV method development, Thomas Laue for guidance in the variable speed analytical ultracentrifugation development, John Philo for providing modified version of the Svedberg software, Marc Kirchmeier and Mohammed Shameem for the support during the development of viscosity, flow cytometry, phase separation, and rat ex vivo bioavailability methods, and Sarah Holtschlag for critical reading of the manuscript.

References

[1] G. Walsh, Biopharmaceuticals: recent approvals and likely directions, Trends Biotechnol. 23 (2005) 553–558.
[2] H.-C. Mahler, W. Friess, U. Grauschopf, S. Kiese, Protein aggregation: pathways, induction factors and analysis, J. Pharm. Sci. 98 (2009) 2909–2934.
[3] S.J. Shire, Z. Shahrokh, J. Liu, Challenges in the development of high protein concentration formulations, Biotechnol.: Pharm. Aspects 11 (2010) 131–147.
[4] A. Saluja, D.S. Kalonia, Nature and consequences of protein–protein interactions in high protein concentration solutions, Int. J. Pharm. 358 (2008) 1–15.
[5] C.-T. Huang, D. Sharma, P. Oma, R. Krishnamurthy, Quantitation of protein particles in parenteral solutions using micro-flow imaging, J. Pharm. Sci. 98 (2009) 3058–3071.
[6] D. Griffiths, P. Hole, J. Smith, B. Carr, Characterization of nanoparticle dispersions by size, scattering intensity simultaneously, Nanotech Conf. Expo 1 (2009) 414–416.
[7] V. Filipe, A. Hawe, W. Jiskoot, Critical evaluation of nanoparticle tracking analysis (NTA) by nanosight for the measurement of nanoparticles and protein aggregates, Pharm. Res. 27 (2010) 796–810.
[8] J.P. Gabrielson, M.L. Brader, A.H. Pekar, K.B. Mathis, G. Winter, J.F. Carpenter, T.W. Randolph, Quantitation of aggregate levels in a recombinant humanized monoclonal antibody formulation by size-exclusion chromatography, asymmetrical flow field flow fractionation, and sedimentation velocity, J. Pharm. Sci. 96 (2006) 268–279.
[9] B. Demeule, C. Palais, G. Machaidze, R. Gurny, T. Arvinte, New methods allowing the detection of protein aggregates: a case study on trastuzumab, MAbs 1 (2009) 142–150.
[10] T. Arakawa, J.S. Philo, D. Ejima, H. Sato, K. Tsumoto, Aggregation analysis of therapeutic proteins, part 3: principles and optimization of field-flow fractionation (FFF), BioProcess Int. 5 (2007) 52. 54, 56, 58, 60–62, 64, 66, 68, 70.
[11] K. Wuchner, J. Buechler, R. Spycher, P. Dalmonte, D.B. Volkin, Development of a microflow digital imaging assay to characterize protein particulates during storage of a high concentration IgG1 monoclonal antibody formulation, J. Pharm. Sci. 99 (2010) 3343–3361.
[12] M.A.H. Capelle, R. Gurny, T. Arvinte, High throughput screening of protein formulation stability: practical considerations, Eur. J. Pharm. Biopharm. 65 (2007) 131–148.
[13] M.A.H. Capelle, R. Gurny, T. Arvinte, High throughput methods to characterize protein permeation and release, Int. J. Pharm. 350 (2008) 272–278.
[14] J.F. Carpenter, T.W. Randolph, W. Jiskoot, D.J.A. Crommelin, C.R. Middaugh, G. Winter, Y.-X. Fan, S. Kirshner, D. Verthelyi, S. Kozlowski, K.A. Clouse, P.G. Swann, A. Rosenberg, B. Cherney, Overlooking subvisible particles in therapeutic protein products: gaps that may compromise product quality, J. Pharm. Sci. 98 (2009) 1201–1205.
[15] S.K. Singh, N. Afonina, M. Awwad, K. Bechtold-Peters, J.T. Blue, D. Chou, M. Cromwell, H.-J. Krause, H.-C. Mahler, B.K. Meyer, L. Narhi, D.P. Nesta, T. Spitznagel, An industry perspective on the monitoring of subvisible particles as a quality attribute for protein therapeutics, J. Pharm. Sci. 99 (2010) 3302–3321.
[16] E.Y. Chi, S. Krishnan, T.W. Randolph, J.F. Carpenter, Physical stability of proteins in aqueous solution: mechanism and driving forces in nonnative protein aggregation, Pharm. Res. 20 (2003) 1325–1336.
[17] T.W. Randolph, E.Y. Chi, S. Krishnan, B.S. Kendrick, J.F. Carpenter. Protein aggregation-conformational stability and colloidal stability, Abstracts of Papers, 224th ACS National Meeting, Boston, MA, United States, August 18–22, 2002 BIOT-160, 2002.
[18] M.E.M. Cromwell, E. Hilario, F. Jacobson, Protein aggregation and bioprocessing, AAPS J. 8 (2006) E572–E579.
[19] C.J. Roberts, Non-native protein aggregation kinetics, Biotechnol. Bioeng. 98 (2007) 927–938.
[20] R. Jaenicke, Protein stability and protein folding, Ciba Found Symposium, vol. 161, pp. 206–216 (discussion pp. 217–221).
[21] Y. Goto, L.J. Calciano, A.L. Fink, Acid-induced folding of proteins, Proc. Natl. Acad. Sci. USA 87 (1990) 573–577.
[22] E. Vazquez-Contreras, P.I. Rodriguez, V. Castillo-Sanchez, M.E. Chanez-Cardenas, The unfolding of proteins induced by different denaturants, Adv. Protein Phys. Chem. (2008) 169–192.
[23] J. Wallach, Stability studies of protein pharmaceuticals, Pharm. Ind. 71 (2009) 687–688. 690–692.
[24] T. Wehr, R. Rodriquez-Diaz, Use of size exclusion chromatography in biopharmaceutical development, Analytical Techniques for Biopharmaceutical Development, Marcel Dekker, Inc., New York, NY, 2005. 95–112.
[25] O.P. Sharma, D.K. Pollo, M.J. Sukumar, Quantification and characterization of subvisible proteinacious particles in opalescent mAb formulations using micro-flow imaging, J. Pharm. Sci. 99 (2010) 2628–2642.
[26] M. Vujtek, R. Kubinek, R. Zboril, The role of atomic force microscopy in nanoparticle research, J. Adv. Microsc. Res. 5 (2010) 67–77.
[27] A. Ikai, A review on: atomic force microscopy applied to nano-mechanics of the cell, Adv. Biochem. Eng./Biotechnol. 119 (2010) 47–61.
[28] R. Creasey, S. Sharma, J.E. Craig, C.T. Gibson, A. Ebner, P. Hinterdorfer, N.H. Voelcker, Detecting protein aggregates on untreated human tissue samples by atomic force microscopy recognition imaging, Biophys. J. 99 (2010) 1660–1667.
[29] K.J. Weronski, P. Cea, I. Diez-Perez, M.A. Busquets, J. Prat, V. Girona, Time-lapse atomic force microscopy observations of the morphology, growth rate, and spontaneous alignment of nanofibers containing a peptide-amphiphile from the hepatitis G virus (NS3 protein), J. Phys. Chem. B 114 (2010) 620–625.
[30] J.C. Johnson, S.R. Nettikadan, S.G. Vengasandra, E.J. Henderson, Analysis of solid-phase immobilized antibodies by atomic force microscopy, Biochem. Biophys. Methods 59 (2004) 167–180.
[31] J. Legleiter, T. Kowalewski, Atomic force microscopy, Protein Rev. 4 (2006) 315–334.
[32] T.J. Smith, Structural studies on antibody-virus complexes, Adv. Protein Chem. 64 (2003) 409–453.
[33] N.H. Thomson, Imaging the substructure of antibodies with tapping-mode AFM in air: the importance of a water layer on mica, J. Microsc. (Oxford, UK) 217 (2005) 193–199.
[34] J.N. Lin, B. Drake, A.S. Lea, P.K. Hansma, J.D. Andrade, Direct observation of immunoglobulin adsorption dynamics using the atomic force microscope, Langmuir 6 (1990) 509–511.

[35] H. Lee, M. Kirchmeier, H. Mach, Monoclonal antibody aggregation intermediates visualized by atomic force microscopy, J. Pharm. Sci. 100 (2011) 416–423.
[36] A.H. Fradkin, J.F. Carpenter, T.W. Randolph, Immunogenicity of aggregates of recombinant human growth hormone in mouse models, J. Pharm. Sci. 98 (2009) 3247–3264.
[37] H.M. Dintzis, R.Z. Dintzis, B. Vogelstein, Molecular determinants of immunogenicity: the immunon model of immune response, Proc. Natl. Acad. Sci. USA 73 (1976) 3671–3675.
[38] A.S. Rosenberg, Effects of protein aggregates: an immunologic perspective, AAPS J. 8 (2006) E501–E507.
[39] S. Hermeling, D.J.A. Crommelin, H. Schellekens, W. Jiskoot, Immunogenicity of therapeutic proteins, Handb. Pharm. Biotechnol. (2007) 815–833.
[40] H. Schellekens, W. Jiskoot, Immunogenicity of therapeutic proteins, Pharm. Biotechnol., third ed., 2008, pp. 125–132.
[41] W. Jiskoot, E.C. Beuvery, A.A.M. De Koning, J.N. Herron, D.J.A. Crommelin, Analytical approaches to the study of monoclonal antibody stability, Pharm. Res. 7 (1990) 1234–1241.
[42] T. Arvinte, Analytical methods for protein formulations, in: W. Jiskootand, D.J.A. Crommelin (Eds.), Methods for Structural Analysis of Protein Pharmaceuticals, AAPS Press, Arlington, VA, 2005, pp. 661–666.
[43] S.J. Shire, J.J. Liu, Development of high protein concentration pharmaceuticals for SC delivery: fitting all the pieces together, Abstracts of Papers, 239th ACS National Meeting, San Francisco, CA, United States, 2010, pp. BIOT-132.
[44] S. Kanai, J. Liu, T.W. Patapoff, S.J. Shire, Reversible self-association of a concentrated monoclonal antibody solution mediated by Fab–Fab interaction that impacts solution viscosity, J. Pharm. Sci. 97 (2008) 4219–4227.
[45] R.P. Haughland, Handbook of Fluorescence Probes and Research Products, Sixth ed., Molecular Probes, Eugene, OR, 1996.
[46] B. Demeule, R. Gurny, T. Arvinte, Detection and characterization of protein aggregates by fluorescence microscopy, Int. J. Pharm. 329 (2007) 37–45.
[47] A. Hawe, M. Sutter, W. Jiskoot, Extrinsic fluorescent dyes as tools for protein characterization, Pharm. Res. 25 (2008) 1487–1499.
[48] W. Jiskoot, A. Hawe, Aggregates enlightened: fluorescent dyes for detecting protein aggregates, BIOforum Eur. 13 (2009) 26–27.
[49] P. Greenspan, S.D. Fowler, Spectrofluorometric studies of the lipid probe, Nile Red, J. Lipid Res. 26 (1985) 781–789.
[50] D.L. Sackett, J.R. Knutson, J. Wolff, Hydrophobic surfaces of tubulin probed by time-resolved and steady-state fluorescence of Nile Red, J. Biol. Chem. 265 (1990) 14899–14906.
[51] H.H. Bauer, A.F. Drake, H.P. Merkle, T. Arvinte, Fluorescence study of human calcitonin fibrillation kinetics using the hydrophobic probe Nile Red, in: Peptides 1992, Proceedings of the 22nd European Peptide Symposium, 1993, pp. 505–506.
[52] Y. Li, H. Mach, J.T. Blue, High-throughput screening of monoclonal antibody aggregation behaviors, Abstracts of Papers, 239th ACS National Meeting, San Francisco, CA, United States, March 21–25, 2010, BIOT-558, 2010.
[53] A. Hawe, W. Friess, M. Sutter, W. Jiskoot, Online fluorescent dye detection method for the characterization of immunoglobulin G aggregation by size exclusion chromatography and asymmetrical flow field flow fractionation, Anal. Biochem. 378 (2008) 115–122.
[54] M.A.H. Capelle, P. Brugger, T. Arvinte, Spectroscopic characterization of antibodies adsorbed to aluminium adjuvants: correlation with antibody vaccine immunogenicity, Vaccine 23 (2005) 1686–1694.
[55] B. Demeule, R. Gurny, T. Arvinte, Detection, characterization of protein aggregates by fluorescence microscopy, Int. J. Pharm. 329 (2007) 37–45.
[56] A. Supersaxo, W.R. Hein, H. Steffen, Effect of molecular weight on the lymphatic absorption of water-soluble compounds following subcutaneous administration, Pharm. Res. 7 (1990) 167–169.
[57] S.A. Charman, A.M. Segrave, G.A. Edwards, C.J. Porter, Systemic availability, lymphatic transport of human growth hormone administered by subcutaneous injection, J. Pharm. Sci. 89 (2005) 168–177.
[58] C.J. Porter, S.A. Charman, Lymphatic transport of proteins after subcutaneous administration, J. Pharm. Sci. 89 (2009) 297–310.
[59] J. Brange, D.R. Owens, S. Kang, A. Volund, Monomeric insulins, their experimental, clinical implications, Diabetes Care 13 (1990) 23–54.
[60] E. Fernqvist, B. Linde, J. Ostman, R. Gunnarsson, Effects of physical exercise on insulin absorption in insulin-dependent diabetics. A comparison between human and porcine insulin, Clin. Physiol. 6 (1986) 489–497.
[61] B. Linde, Dissociation of insulin absorption and blood flow during massage of a subcutaneous injection site, Diabetes Care 9 (1986) 570–574.
[62] H. Mach, S. Gregory, S. Mittal, A. Lalloo, M. Kirchmeier, M. Shameem, Electrostatic interactions of monoclonal antibodies with subcutaneous tissue, Ther. Deliv., in press.
[63] T. Ahamed, B.K. Nfor, P.D.E.M. Verhaert, G.W.K. Van Dedem, L.A.M. van der Wielen, M.H.M. Eppink, E.J.A.X. van de Sandt, M. Ottens, pH-gradient ion-exchange chromatography: an analytical tool for design and optimization of protein separations, J. Chromatogr. A 1164 (2007) 181–188.
[64] D. Daitoku, T. Kurose, E. Mori, M. Hashimoto, S. Kawamata, Changes in the rat subcutaneous connective tissue after saline and histamine injection in relation to fluid storage and excretion, Arch. Histol. Cytol. 70 (2007) 29–41.
[65] L.H. Bookbinder, A. Hofer, M.F. Haller, M.L. Zepeda, G.A. Keller, J.E. Lim, T.S. Edgington, H.M. Shepard, J.S. Patton, G.I. Frost, A recombinant human enzyme for enhanced interstitial transport of therapeutics, J. Controlled Release 114 (2006) 230–241.
[66] XolairR, Prescribing information, www.xolair.com/prescribing_information.html.
[67] T.A. Waldmann, W. Strober, Metabolism of immunoglobulins, Progr. Allergy 13 (1969) 1–110.
[68] W.E. Wang, J.P. Balthasar, Monoclonal antibody pharmacokinetics and pharmacodynamics, Clin. Pharm. Ther. 84 (2008) 548–558.
[69] R.P. Junghans, Finally! The Brambell receptor (FcRB). Mediator of transmission of immunity and protection from catabolism for IgG, Immunol. Res. 16 (1997) 29–57.
[70] H. Mach, C.R. Middaugh, R.V. Lewis, Statistical determination of the average values of the extinction coefficients of tryptophan, tyrosine in native proteins, Anal. Biochem. 200 (1992) 74–80.
[71] C.N. Pace, F. Vajdos, L. Fee, G. Grimsley, T. Gray, How to measure, predict the molar absorption coefficient of a protein, Protein Sci. 4 (1995) 2411–2423.
[72] H. Mach, C.R. Middaugh, Ultraviolet spectroscopy as a tool in therapeutic protein development, J. Pharm. Sci. 100 (2011) 1214–1227.
[73] I. Oreskes, D. Mandel, Spectrophotometric assay with turbidity correction of sized immunoglobulin G aggregates, Anal. Biochem. 99 (1979) 346–351.
[74] A.F. Winder, W.L.G. Gent, Correction of light-scattering errors in spectrophotometric protein determinations, Biopolymers 10 (1971) 1243–1251.
[75] A. Bootz, V. Vogel, D. Schubert, J. Kreuter, Comparison of scanning electron microscopy, dynamic light scattering and analytical ultracentrifugation for the sizing of poly(butyl cyanoacrylate) nanoparticles, Eur. J. Pharm. Biopharm. 57 (2004) 369–375.
[76] H. Mach, A. Bhambhani, B.K. Meyer, S. Burek, H. Davis, J.T. Blue, R.K. Evans, The use of flow cytometry for the detection of therapeutic protein aggregates, J. Pharm. Sci. 100 (2011) 1671–1678.
[77] D.B. Ludwig, J.T. Trotter, J.P. Gabrielson, J.F. Carpenter, T.W. Randolph, Flow cytometry: a promising technique for the study of silicone oil-induced particulate formation in protein formulations, Anal. Biochem. 410 (2011) 191–199.
[78] F. He, D.H. Phan, S. Hogan, R. Bailey, G.W. Becker, L.O. Narhi, V.I. Razinkov, Detection of IgG aggregation by a high throughput method based on extrinsic fluorescence, J. Pharm. Sci. 99 (2010) 2598–2608.
[79] F. He, S. Hogan, R.F. Latypov, L.O. Narhi, V.I. Razinkov, High throughput thermostability screening of monoclonal antibody formulations, J. Pharm. Sci. 99 (2010) 1707–1720.
[80] M.D. Cummings, M.A. Farnum, M.I. Nelen, Universal screening methods, applications of thermofluor, J. Biomol. Screen. 1 (2006) 854–863.
[81] U.B. Ericsson, B.M. Hallberg, G.T. DeTitta, N. Dekker, P. Nordlund, Thermofluor-based high-throughput stability optimization of proteins for structural studies, Anal. Biochem. 357 (2006) 289–298.
[82] M.E.M. Cromwell, J.F. Carpenter, T. Scherer, T.W. Randolph, Opalescence in antibody formulations is a solution critical phenomenon, Abstracts of Papers, 236th ACS National Meeting, Philadelphia, PA, United States, BIOT-029, 2008.
[83] N. Taschner, S.A. Mueller, V.R. Alumalla, K.N. Goldie, A.F. Drake, U. Aebi, T. Arvinte, Modulation of antigenicity related to changes in antibody flexibility upon lyophilization [erratum to document cited in CA136:107411], J. Mol. Biol. 312 (2001) 579.
[84] B.A. Salinas, H.A. Sathish, S.M. Bishop, N. Harn, J.F. Carpenter, T.W. Randolph, Understanding and modulating opalescence and viscosity in a monoclonal antibody formulation, J. Pharm. Sci. 99 (2009) 82–93.
[85] H. Zimmer, Viscosity and viscosity measurements, Allgem. Osterr. Chem. U. Tech.-Ztg. 50 (1932) 47–50.
[86] U. Teipel, A.C. Hordijk, U. Foerter-Barth, D.M. Hoffman, C. Huebner, V. Valtsifer, K.E. Newman, Rheology, Energ. Mater. (2005) 433–508.
[87] P.T. Reardon, A.L. Graham, S. Feng, V. Chawla, R.S. Admuthe, L.A. Mondy, Non-Newtonian end effects in falling ball viscometry of concentrated suspensions, Rheol. Acta 46 (2007) 413–424.
[88] F. He, G.W. Becker, J.R. Litowski, L.O. Narhi, D.N. Brems, V.I. Razinkov, High-throughput dynamic light scattering method for measuring viscosity of concentrated protein solutions, Anal. Biochem. 399 (2010) 141–143.
[89] S.P. Sutera, R. Skalak, The history of Poiseuille's law, Annu. Rev. Fluid Mech. 25 (1993) 1–19.
[90] N.-S. Chang, Formula for the viscosity of a glycerol–water mixture, Ind. Eng. Chem. Res. 47 (2008) 3285–3288.
[91] M.S. Runge, T.M. Laue, D.A. Yphantis, M.R. Lifsics, A. Saito, M. Altin, K. Reinke, R.C. Williams Jr., ATP-induced formation of an associated complex between microtubules and neurofilaments, Proc. Natl. Acad. Sci. USA 78 (1981) 1431–1435.
[92] W. Machtle, High-resolution, submicron particle size distribution analysis using gravitational-sweep sedimentation, Biophys. J. 76 (1999) 1080–1091.
[93] H. Mach, D.B. Volkin, R.D. Troutman, B. Wang, Z. Luo, K.U. Jansen, L. Shi, Disassembly and reassembly of yeast-derived recombinant human papillomavirus virus-like particles (HPV VLPs), J. Pharm. Sci. 95 (2006) 2195–2206.
[94] W.F. Stafford, E.H. Braswell, Sedimentation velocity multi-speed method for analyzing polydisperse solutions, Biophys. Chem. 108 (2004) 273–279.
[95] B. Demeule, M.J. Lawrence, A.F. Drake, R. Gurny, T. Arvinte, Characterization of protein aggregation: the case of a therapeutic immunoglobulin, Biochim. Biophys. Acta-Proteins and Proteomics 1774 (2007) 146–153.
[96] J.F. Carpenter, T.W. Randolph, W. Jiskoot, D.J.A. Crommelin, C.R. Middaugh, G. Winter, Potential inaccurate quantitation and sizing of protein aggregates by

size exclusion chromatography: essential need to use orthogonal methods to assure the quality of therapeutic protein products, J. Pharm. Sci. 99 (2010) 2200–2208.
[97] B. Demeule, S.J. Shire, J. Liu, Challenges in protein formulation: sub-visible particles characterization, Abstracts of Papers, 239th ACS National Meeting, San Francisco, CA, United States, March 21–25, BIOT-136, 2010.
[98] T. Arvinte, Formulation of protein drugs – important points to consider, BioWorld Eur. 01 (2007) 6–9.
[99] J.S. Philo, Improved methods for fitting sedimentation coefficient distributions derived by time-derivative techniques, Anal. Biochem. 354 (2006) 238–246.
[100] J.S. Philo, Analytical ultracentrifugation, Biotechnol.: Pharm. Aspects 3 (2005) 379–412.